The Run-2 ATLAS Trigger System

Arantxa Ruiz Martínez on behalf of the ATLAS Collaboration
Department of Physics, Carleton University, Ottawa, ON, Canada
E-mail: aranzazu.ruiz.martinez@cern.ch

Abstract. The ATLAS trigger successfully collected collision data during the first run of the LHC between 2009-2013 at different centre-of-mass energies between 900 GeV and 8 TeV. The trigger system consists of a hardware Level-1 and a software-based high level trigger (HLT) that reduces the event rate from the design bunch-crossing rate of 40 MHz to an average recording rate of a few hundred Hz. In Run-2, the LHC will operate at centre-of-mass energies of 13 and 14 TeV and higher luminosity, resulting in up to five times higher rates of processes of interest. A brief review of the ATLAS trigger system upgrades that were implemented between Run-1 and Run-2, allowing to cope with the increased trigger rates while maintaining or even improving the efficiency to select physics processes of interest, will be given. This includes changes to the Level-1 calorimeter and muon trigger systems, the introduction of a new Level-1 topological trigger module and the merging of the previously two-level HLT system into a single event processing farm. A few examples will be shown, such as the impressive performance improvements in the HLT trigger algorithms used to identify leptons, hadrons and global event quantities like missing transverse energy. Finally, the status of the commissioning of the trigger system and its performance during the 2015 run will be presented.

ATL-DAQ-PROC-2016-003
28/02/2016

1. Introduction

The trigger system is an essential component of the ATLAS [1] experiment at the LHC [2], since it is responsible for deciding whether or not to keep a given collision event for later study. In the LHC Run-1 (2009-2013), the ATLAS trigger system [3] operated efficiently at instantaneous luminosities of up to $8 \times 10^{33}\,\mathrm{cm}^{-2}\mathrm{s}^{-1}$ at different centre-of-mass energies between 900 GeV and 8 TeV and collected more than three billion events. In the LHC Run-2, which started in 2015, the increased collision energy to 13 TeV, higher luminosity and higher pile-up lead to an increase of the rates as compared to the Run-1 trigger selections by up to a factor five, exceeding the capabilities of the Run-1 trigger system. The LHC long shutdown (2013-2014) was therefore used to perform major upgrades in the different components of the trigger system.

2. The ATLAS Trigger System Upgrades for Run-2

The trigger system in Run-2 consists of a hardware-based first level trigger (Level-1) [4] and a software-based high level trigger (HLT) [5]. The Level-1 trigger uses custom electronics to determine Regions-of-Interest (RoIs) in the detector, taking as input coarse granularity calorimeter and muon detector information. The Level-1 trigger reduces the event rate from the LHC bunch crossing rate of approximately 30 MHz to 100 kHz. The decision time for a Level-1 accept is 2.5 μs. The RoIs formed at Level-1 are sent to the HLT in which sophisticated selection algorithms are run using full granularity detector information in either the RoI or the whole event. The HLT reduces the rate from the Level-1 output rate of 100 kHz to approximately

1 kHz on average within a processing time of about 200 ms. A schematic overview of the upgraded ATLAS trigger and data acquisition system is shown in Fig. 1.

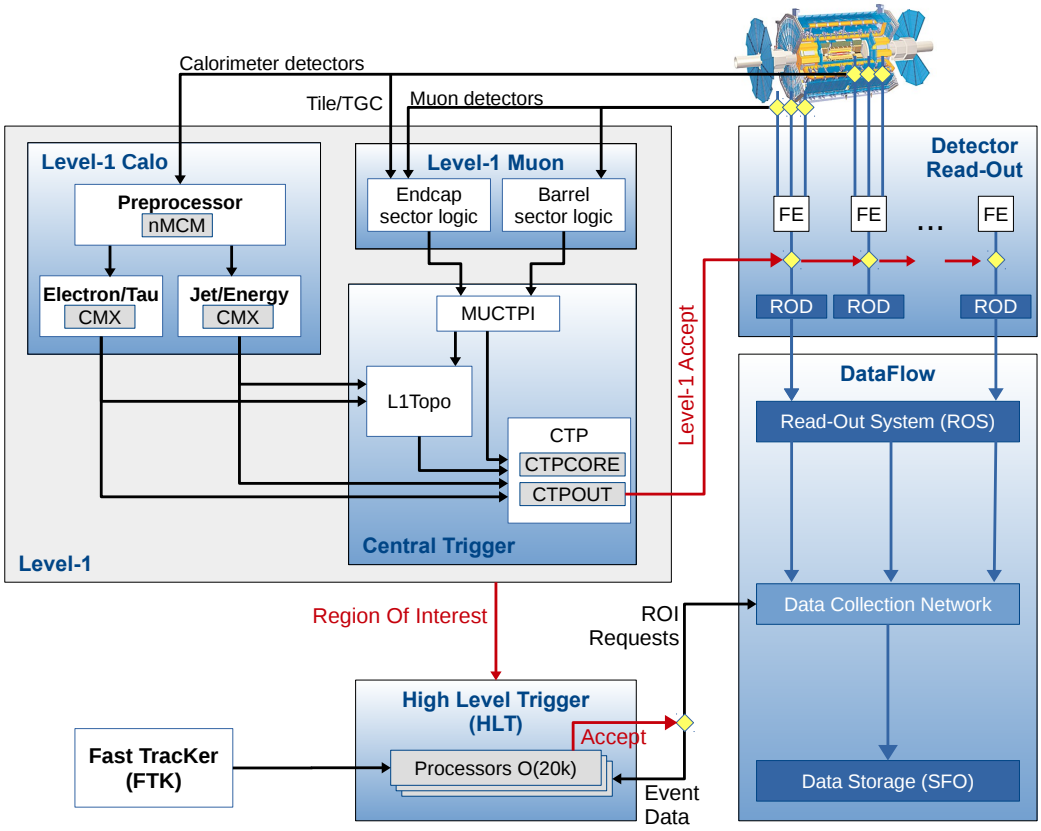

Figure 1. Schematic layout of the ATLAS trigger and data acquisition system in Run-2.

2.1. Level-1 Trigger Upgrades

Several upgrades have been introduced in the different components of the ATLAS Level-1 trigger system for Run-2 data taking. The upgrades, both in the Level-1 trigger hardware and in the detector readout, allowed to rise the maximum Level-1 trigger rate from 70 kHz in Run-1 to 100 kHz in Run-2.

The Level-1 Calorimeter trigger makes use of reduced granularity information from the electromagnetic and hadronic calorimeters to search for electrons, photons, taus and jets, as well as high total and missing transverse energy ($E_{\mathrm{T}}^{\mathrm{miss}}$). One of the main upgrades in the Level-1 Calorimeter trigger is the new Multi-Chip Modules (nMCM), based on field-programmable gate array (FPGA) technology, which replace the application-specific integrated circuits (ASICs) included in the modules used in Run-1. This new hardware allows the use of auto-correlation filters and a new bunch-by-bunch dynamic pedestal correction, meant to suppress pile-up effects. The effect of these corrections in linearising the $E_{\mathrm{T}}^{\mathrm{miss}}$ trigger rates as function of the instantaneous luminosity is illustrated in Fig. 2.

The Level-1 Muon trigger system, which consists of a barrel section and two endcap sections, provides fast trigger signals from the muon detectors for the Level-1 trigger decision. For Run-2, various improvements were added to the Level-1 Muon trigger. To suppress most of the fake

muon triggers, the muon endcap trigger ($1.05 < |\eta| < 2.4$)[1] now requires a coincidence with hits from the innermost muon chambers (known as Forward Inner, FI), which as shown in Fig. 3 reduces the L1_MU15 rate by approximately 50% in the $1.3 < |\eta| < 1.9$ region with a very small signal efficiency loss of only ∼2%. The L1_MU15 trigger requires that a candidate passed the 15 GeV threshold requirement of the Level-1 muon trigger system. In the future, a similar coincidence logic will also be applied using the outermost layer of the hadronic Tile Calorimeter for $1.05 < |\eta| < 1.3$. Moreover, the trigger coverage is expected to be improved by 4% in the barrel region due to the installation of new chambers in the feet region of the muon detector, which are currently being commissioned.

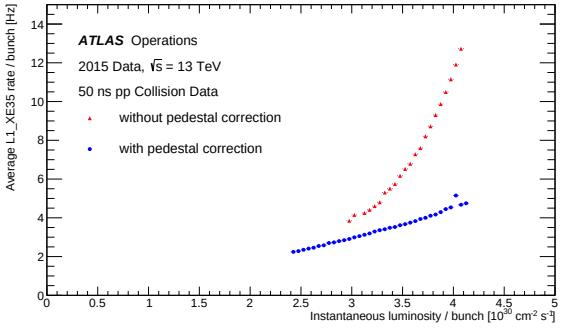

Figure 2. Trigger rate per bunch for an $E_{\mathrm{T}}^{\mathrm{miss}}$ trigger with a threshold at 35 GeV as function of the instantaneous bunch luminosity with and without Level-1 Calorimeter pedestal correction applied [6].

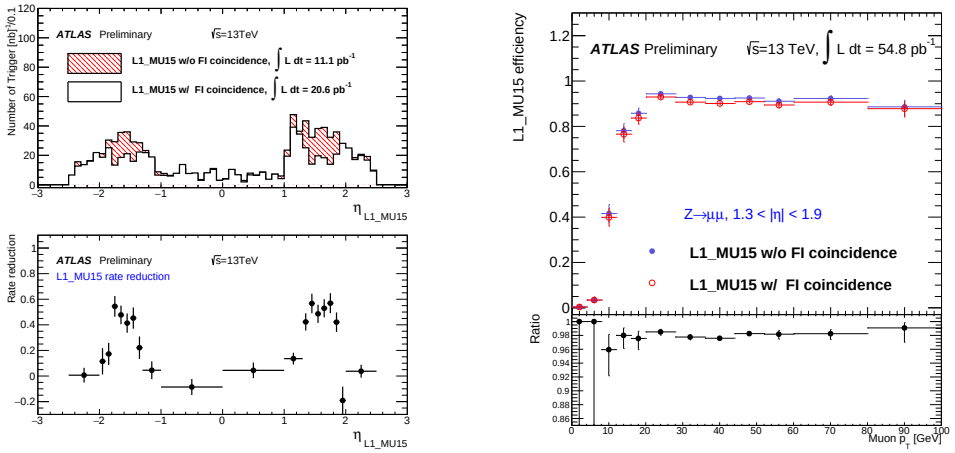

Figure 3. Distribution of the RoI η from the L1_MU15 trigger with and without the FI coincidence enabled (top left), and reduction of the trigger rate due to this coincidence (bottom left) [7]. On the right, the efficiency of the L1_MU15 trigger in the endcap region with and without the FI coincidence enabled [7].

[1] ATLAS uses a right-handed coordinate system with its origin at the nominal interaction point (IP) in the centre of the detector and the z-axis along the beam pipe. The x-axis points from the IP to the centre of the LHC ring, and the y-axis points upward. Cylindrical coordinates (r, ϕ) are used in the transverse plane, ϕ being the azimuthal angle around the z-axis. The pseudorapidity is defined in terms of the polar angle θ as $\eta = -\ln\tan(\theta/2)$.

A new topological trigger processor (L1Topo) has been deployed for Run-2 and is currently under commissioning. It takes as input the Level-1 trigger objects from the output merger modules (CMX) of the Level-1 Calorimeter trigger and the Level-1 Muon trigger (MuCTPi), which were both also upgraded. The new L1Topo system allows to apply topological selections at the Level-1 trigger combining kinematic information from multiple calorimeter and muon trigger objects, such as angular separation, invariant mass requirements, or global event quantities such as the sum of the transverse momenta of all Level-1 jet objects. The use of L1Topo significantly suppresses backgrounds for many trigger selections, in many cases by more than a factor of two, allowing to preserve the sensitivity for channels such as $B_s \to \mu\mu$ and $H \to \tau\tau$ at the current level with increasing luminosity.

The central trigger processor (CTP) forms the Level-1 trigger decision based on the information received from the L1Topo, Level-1 Calorimeter trigger and Level-1 Muon trigger, and distributes the Level-1 accept signal and LHC timing signals to the sub-detector readout systems via the Timing, Trigger and Control network. The main part of the CTP was replaced to increase the number of trigger inputs and trigger items, achieving more flexibility in the selection of events relevant for physics analyses. These improvements required the upgrade of the hardware or firmware of most CTP components, as well as a complete re-design of its software architecture.

The Fast TracKer (FTK) [8] project is a fast hardware-based tracking system designed to perform a global track reconstruction receiving input from the ATLAS silicon tracking detectors after each Level-1 trigger and provides full-event track information to the HLT. This can be used to improve many trigger selections requiring full-event tracking information, like b-jets, which would not be otherwise affordable at HLT. In addition the precise estimation of the pile-up conditions per event can be used to develop pile-up robust trigger strategies. With the Run-2 data taking ongoing, the first boards of FTK are being installed, already reading ATLAS data in parasitic mode. The full deployment and operation of the barrel region is expected for mid 2016, after which the integration within HLT and the extension to full coverage will follow.

The minimum bias trigger scintillators (MBTS) provided the primary trigger for selecting events from low luminosity proton-proton and lead-lead collisions with the smallest possible bias. Due to the radiation damage the MBTS have been replaced during the LHC long shutdown and are mounted at each end of the detector in front of the liquid-argon end-cap calorimeter cryostats at $z = \pm 3.56\,\mathrm{m}$ and segmented into two rings in pseudorapidity ($2.07 < |\eta| < 2.76$ and $2.76 < |\eta| < 3.86$). The inner ring is segmented into eight azimuthal sectors while the outer ring is segmented into four azimuthal sectors, giving a total of twelve sectors per side.

2.2. High Level Trigger Upgrades

There have also been significant upgrades in the HLT during the LHC long shutdown. In Run-1 the ATLAS trigger system had separate Level-2 and Event Filter computer clusters. For Run-2, the system has been merged into a single event processing HLT farm, which reduces the complexity and allows for dynamic resource sharing between algorithms. This new arrangement reduces code and algorithm duplication and results in a more flexible HLT, reducing duplicated data-fetching.

Most of the trigger reconstruction algorithms were re-optimized during the shutdown to minimize differences between the HLT and the offline analysis selections, which in some cases, such as in the hadronic tau triggers, reduced inefficiencies by more than a factor two. The HLT tracking algorithms have also been prepared for the future inclusion of the FTK. The HLT processing performed within RoIs has been augmented for some triggers to also allow aggregation of the RoIs into a single object. This reduces the amount of CPU processing required for events with a large multiplicity of partially overlapping RoIs. The average output rate of the HLT has been increased from 400 Hz to 1 kHz, as imposed by data storage constraints.

3. ATLAS Trigger System Commissioning and Performance in Run-2

The ATLAS trigger system has been successfully commissioned in the start-up phase of Run-2 with cosmic ray data and early $\sqrt{s} = 13\,\text{TeV}$ collision data. Most of the new trigger components have been used during the 2015 data taking period, allowing ATLAS to efficiently select events in Run-2. In this section, the efficiencies of the main physics triggers in the initial phase of Run-2 and comparisons to Monte Carlo (MC) simulations are discussed.

Photons are triggered using a cut-based identification criteria with different selections available (loose, medium and tight) [9]. The efficiency of several single photon triggers is shown in Fig. 4 with respect to photon candidates reconstructed using the full ATLAS reconstruction software passing a tight identification selection. The efficiency is measured as a function of the offline photon transverse energy for $|\eta| < 2.37$ excluding the transition region between the barrel and endcap electromagnetic calorimeters at $1.37 < |\eta| < 1.52$, using events recorded with a Level-1 trigger requiring an electromagnetic energy cluster with $E_{\text{T}} > 7\,\text{GeV}$.

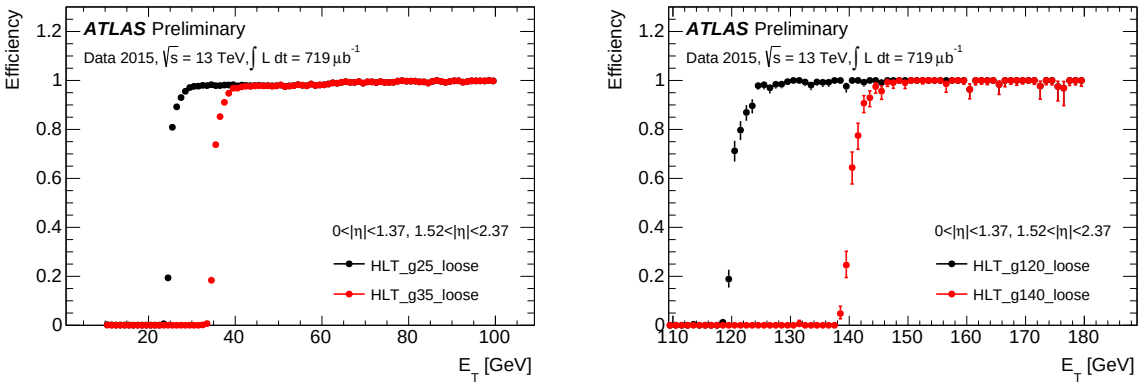

Figure 4. Efficiency for the single photon triggers requiring $E_{\text{T}} > 25\,\text{GeV}$ and $35\,\text{GeV}$ (left), and requiring $E_{\text{T}} > 120\,\text{GeV}$ and $140\,\text{GeV}$ (right) as a function of the E_{T} of the offline photon candidates [10]. Only statistical uncertainties are shown.

Electrons are selected at the HLT using a likelihood-based identification criteria which takes as input electromagnetic shower shape and tracking information with different selections available (lhloose, lhmedium and lhtight) [11]. Figure 5 shows the efficiency of the combined Level-1 and HLT single electron e12_lhloose_L1EM10VH and e24_lhmedium_L1EM20VH triggers as a function of the E_{T} of the offline electron candidates. These triggers require an electron candidate with $E_{\text{T}} > 12\,\text{GeV}$ satisfying the lhloose identification, and $E_{\text{T}} > 24\,\text{GeV}$ satisfying the lhmedium identification, respectively. They are seeded by the Level-1 triggers L1_EM10VH and L1_EM20VH, respectively, that apply an E_{T} dependent veto against energy deposited in the hadronic calorimeter behind the electron candidates electromagnetic cluster. The efficiency is measured with a tag-and-probe method using $Z \to ee$ decays and compared to the expectation from $Z \to ee$ MC simulation.

Muons are reconstructed at the HLT by combining the inner detector and muon spectrometer tracks. The absolute efficiency of the L1_MU15 trigger and absolute and relative efficiencies of the OR combination of mu20_iloose and mu50 HLT triggers are shown in Fig. 6 as a function of the p_{T} of the offline muon candidates in the barrel and endcap detector regions. The efficiency is computed with respect to the offline muon candidates requiring to pass a medium quality requirement defined in Ref. [12]. The L1_MU15 trigger requires that a candidate passed the 15 GeV threshold requirement of the Level-1 muon trigger system. The mu20_iloose trigger is seeded by the L1_MU15 trigger and is required to satisfy a 20 GeV HLT threshold and to pass a

loose isolation selection computed using inner detector tracks reconstructed online by the HLT. The mu50 trigger is seeded by the L1_MU20 trigger and is required to satisfy a 50 GeV HLT threshold. The efficiency is measured with a tag-and-probe method using $Z \to \mu\mu$ candidates. The Level-1 trigger efficiency of ∼70% observed in the barrel region is mainly due to the detector geometrical acceptance.

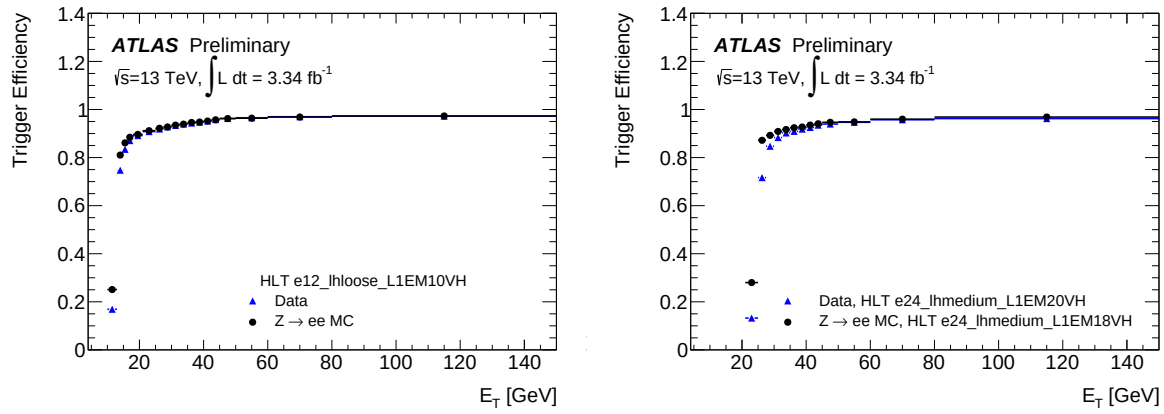

Figure 5. Efficiency for single electron triggers requiring $E_{\mathrm{T}} > 12\,\mathrm{GeV}$ (left) and $E_{\mathrm{T}} > 24\,\mathrm{GeV}$ (right) as a function of the E_{T} of the offline electron candidates. Results are shown for data and $Z \to ee$ MC simulation [10]. Combined statistical and systematic uncertainties are shown.

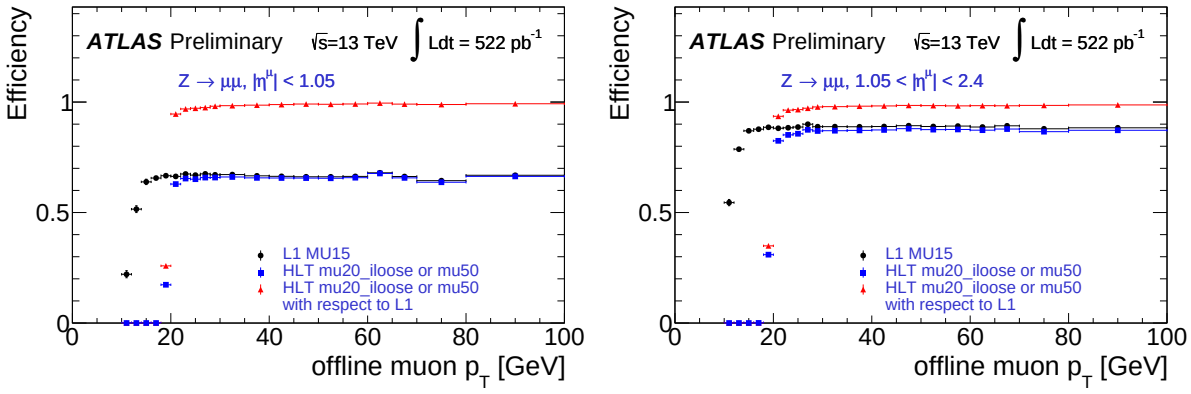

Figure 6. Efficiency for single muon triggers as function of the p_{T} of the offline muon candidates in the barrel (left) and endcap (right) regions [13]. Only statistical uncertainties are shown.

Tau candidates are identified at the HLT using a boosted decision tree (BDT) built from calorimeter and track quantities using different working points (loose, medium and tight) [14]. Figure 7 shows the BDT score and the tau trigger efficiency measured in a data sample enriched in $Z \to \tau\tau \to \mu\tau_{\mathrm{had}}$ events and compared to MC simulation. The efficiency is computed with respect to offline reconstructed tau candidates with $p_{\mathrm{T}} > 25\,\mathrm{GeV}$, one or three tracks and passing the offline medium identification requirement. The corresponding online tau candidate is required to have $p_{\mathrm{T}} > 25\,\mathrm{GeV}$, between one and three tracks and pass the online medium identification requirement.

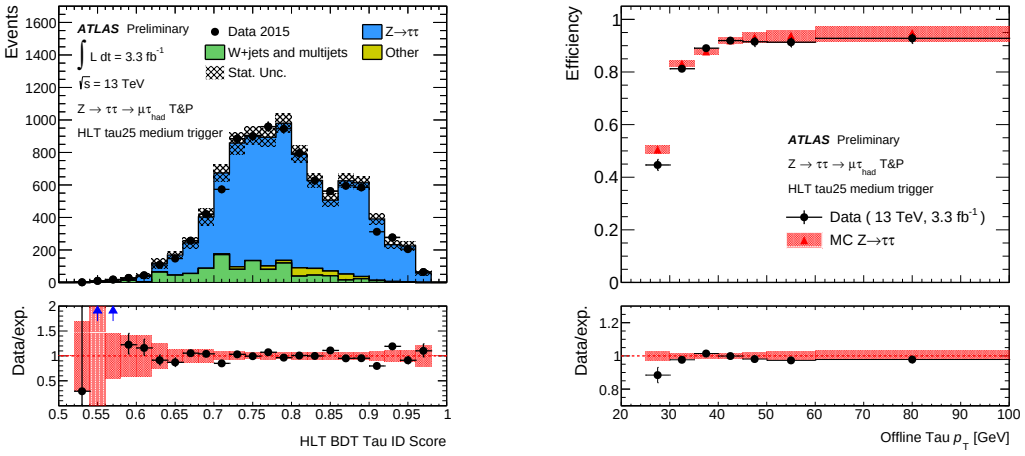

Figure 7. BDT tau identification score for online tau candidates passing the HLT tau trigger with $p_{\mathrm{T}} > 25\,\mathrm{GeV}$ and online medium identification requirement (left) and the corresponding trigger efficiency as function of the p_{T} of the offline tau candidates (right) [15]. Only statistical uncertainties are shown.

HLT jets are formed from topological energy clusters [16] at the electromagnetic energy scale. The HLT jets are then calibrated to the hadronic scale by first applying a jet-by-jet area subtraction procedure followed by a jet energy scale weighting that is dependent on the HLT jet p_{T} and η [17]. The per-event trigger efficiency turn-on curves compared between data and MC simulation for three typical thresholds are shown in Fig. 8. Each efficiency is determined using events retained with a lower threshold trigger that is found to be fully efficient in the phase space of interest.

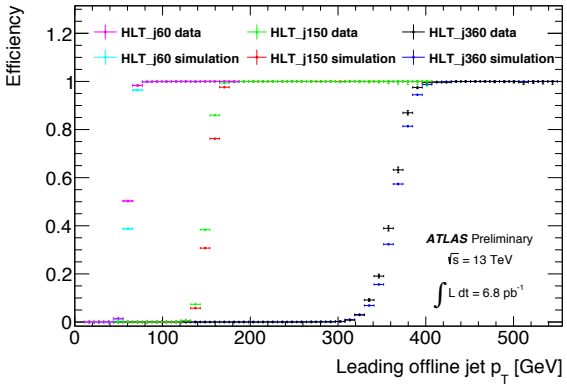

Figure 8. Efficiency for different single jet triggers as function of the offline leading jet p_{T} measured in data and MC simulation [18].

In the $E_{\mathrm{T}}^{\mathrm{miss}}$ trigger, one of the main challenges is the pile-up mitigation. Therefore, different approaches have been studied: cell-based (default), jet-based (mht), and topocluster-based algorithms with (tc_PS) and without (tc) a pile-up subtraction scheme. Figure 9 shows the $E_{\mathrm{T}}^{\mathrm{miss}}$ trigger efficiency turn-on curves with respect to the $E_{\mathrm{T}}^{\mathrm{miss}}$ reconstructed offline without muon corrections. The dataset has been selected using the lowest unprescaled single muon trigger and

events are also required to satisfy a $W \to \mu\nu$ selection. The different turn-on curves have been obtained for the lowest unprescaled trigger of various HLT $E_{\mathrm{T}}^{\mathrm{miss}}$ algorithms for a constant HLT threshold of 70 GeV activated during the 25 ns runs and for different HLT thresholds leading to the same trigger rate.

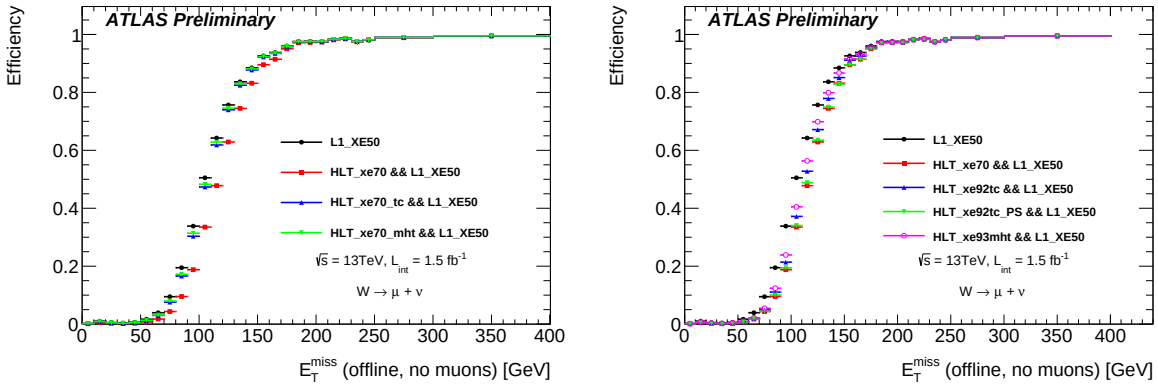

Figure 9. Efficiency for $E_{\mathrm{T}}^{\mathrm{miss}}$ triggers with respect to the $E_{\mathrm{T}}^{\mathrm{miss}}$ reconstructed offline for the different HLT algorithms with a constant HLT threshold (left) and with an equal trigger rate (right) [19]. Only statistical uncertainties are shown.

4. Conclusions

Many improvements have been deployed in the ATLAS trigger system during the LHC shutdown to keep trigger thresholds as low as possible and selections close to the full reconstruction procedure. Some of these improvements include upgrades in the Level-1 Calorimeter and Muon trigger systems, a new Level-1 topological trigger and an upgraded Level-1 central trigger. The HLT architecture has been unified and thus became more performant and flexible.

The trigger system has been successfully commissioned with 2015 data. The first performance studies of the different trigger signatures have been presented using Run-2 $\sqrt{s} = 13$ TeV data.

References

[1] ATLAS Collaboration 2008 *JINST* **3** S08003.
[2] L. Evans and P. Bryant (editors) 2008 *JINST* **3** S08001.
[3] ATLAS Collaboration 2012 *Eur. Phys. J. C* **72** 1849.
[4] ATLAS Collaboration 1998 CERN-LHCC-98-014 http://cdsweb.cern.ch/record/381429.
[5] ATLAS Collaboration 2003 CERN-LHCC-2003-022 http://cdsweb.cern.ch/record/616089.
[6] https://twiki.cern.ch/twiki/bin/view/AtlasPublic/L1CaloTriggerPublicResults.
[7] https://twiki.cern.ch/twiki/bin/view/AtlasPublic/L1MuonTriggerPublicResults.
[8] ATLAS Collaboration 2013 CERN-LHCC-2013-007 http://cdsweb.cern.ch/record/1552953.
[9] ATLAS Collaboration 2012 ATLAS-CONF-2012-123 http://cdsweb.cern.ch/record/1473426.
[10] https://twiki.cern.ch/twiki/bin/view/AtlasPublic/EgammaTriggerPublicResults.
[11] ATLAS Collaboration 2015 ATL-PHYS-PUB-2015-041 http://cdsweb.cern.ch/record/2048202.
[12] ATLAS Collaboration 2015 ATL-PHYS-PUB-2015-037 http://cdsweb.cern.ch/record/2047831.
[13] https://twiki.cern.ch/twiki/bin/view/AtlasPublic/MuonTriggerPublicResults.
[14] ATLAS Collaboration 2015 ATL-PHYS-PUB-2015-045 http://cdsweb.cern.ch/record/2064383.
[15] https://twiki.cern.ch/twiki/bin/view/AtlasPublic/TauTriggerPublicResults.
[16] W. Lampl *et al.* 2008 ATL-LARG-PUB-2008-002 http://cdsweb.cern.ch/record/1099735.
[17] ATLAS Collaboration 2015 ATL-PHYS-PUB-2015-015 http://cdsweb.cern.ch/record/2037613.
[18] https://twiki.cern.ch/twiki/bin/view/AtlasPublic/JetTriggerPublicResults.
[19] https://twiki.cern.ch/twiki/bin/view/AtlasPublic/MissingEtTriggerPublicResults.